

# Sudden End of X-Ray Outbursts around Periastron of Circinus X-1 Observed with MAXI

Kazumi ASAI,<sup>1</sup> Tatehiro MIHARA,<sup>1</sup> Masaru MATSUOKA,<sup>1</sup> Mutsumi SUGIZAKI,<sup>1</sup> Satoshi NAKAHIRA,<sup>2</sup> Hitoshi NEGORO,<sup>3</sup> Motoki NAKAJIMA,<sup>4</sup> and Atsuo T. OKAZAKI<sup>5</sup>

<sup>1</sup>MAXI team, RIKEN, 2-1 Hirosawa, Wako, Saitama 351-0198  
kazumi@crab.riken.jp

<sup>2</sup>ISS Science Project Office, ISAS, JAXA, 2-1-1 Sengen, Tsukuba, Ibaraki 305-8505

<sup>3</sup>Department of Physics, Nihon University, 1-8-14 Kanda-Surugadai, Chiyoda-ku, Tokyo 101-8308

<sup>4</sup>School of Dentistry at Matsudo, Nihon University, 2-870-1 Sakaecho-nishi, Matsudo, Chiba 271-8587

<sup>5</sup>Faculty of Engineering, Hokkai-Gakuen University, Toyohira-ku, Sapporo 062-8605

(Received 2014 March 14; accepted 2014 May 21)

## Abstract

MAXI/GSC observed 21 outbursts from Circinus X-1 between 2009 August and 2013 December. Although 14 outbursts showed ordinary gradual decays, in 7 outbursts we found sudden luminosity decrease in a time scale of a few hours around the periastron, and then the outbursts terminated. These sudden decreases started at the estimated luminosity of a few times  $10^{37}$  erg s<sup>-1</sup> and reached to  $\lesssim 3 \times 10^{36}$  erg s<sup>-1</sup>. We propose three interpretations for the sudden luminosity decrease: (1) the end of the outburst during the dip, (2) the propeller effect, and (3) the stripping effect by the stellar wind of the companion star. It is difficult to explain the phenomenon with any of these interpretations alone. The interpretation of (1) is possible for only two outbursts assuming rapid decay. The propeller effect (2) is expected to occur at a constant luminosity, which is incompatible with the observed facts. In wind stripping effect (3), the ram pressure of a typical stellar wind is not sufficient to blow out most of the accretion disk. In this paper, we discuss a possibility of a modified effect of (3) assuming other additional conditions such as wind clumping and disk instability.

**Key words:** stars: early-type — X-rays: binaries — X-rays: individual (Cir X-1)

## 1. Introduction

Circinus X-1 (hereafter Cir X-1) is a bright X-ray binary located on the Galactic plane. The nature of the large variability in various time scales has not been well understood yet. The source shows a recurrent X-ray activity coupled with an orbital period of 16.6 d (Kaluziński et al. 1976). It is also known to show long-term variabilities on a time-scale of years, and the flux level varies from undetectable levels to more than 1 Crab (Parkinson et al. 2003; Clarkson et al. 2004; Armstrong et al. 2013). When the luminosity is high, it frequently showed X-ray outbursts and radio flares by the 16.6 d orbital cycle. The flaring events are believed to be caused by an increased mass transfer from the companion star near the periastron passage of a highly eccentric binary orbit (Kaluziński et al. 1976; Jonker et al. 2007). The X-ray outbursts are accompanied by absorption dips in the X-ray flux. Clarkson et al. (2004) reported that the X-ray dips would provide more accurate system clock than the maximum of the X-ray outbursts. Recently, periodic radio flares are considered more suitable for defining the orbital motion, and used as the phase zero in the ephemeris (Nicolson 2007).

X-ray spectra observed with ASCA, RXTE, and BeppoSAX during the dips are consistent with a partial covering model of absorbing matter in which the intensity of the intrinsic emission does not change (Brandt et

al. 1996; Shirey et al. 1999b; Iaria et al. 2001a, 2001b).

Observations of Chandra HETGS near periastron have revealed presence of emission lines of H-like and/or He-like Ne, Mg, Si, S, and Fe. These lines are broad and show P Cygni profiles with velocities of  $\pm 2000$  km s<sup>-1</sup> (Brandt & Schulz 2000). These results suggest that a wind with a moderate temperature ( $\sim 5 \times 10^6$  K) from the X-ray-heated accretion disk is responsible for the P Cygni profiles.

Cir X-1 does not fit the conventional classification of X-ray binaries, either HMXBs (high-mass X-ray binaries) or LMXBs (low-mass X-ray binaries) (White 1989). In addition to type-I X-ray bursts (Tennant et al. 1986; Linares et al. 2010), spectral and timing features revealing both Z-source and atoll-source (Shirey et al. 1999a; Soleri et al. 2009) and rapid variability with kHz quasi-periodic oscillations (Boutloukos et al. 2006) agree with a typical behaviors in LMXBs embedding a weakly magnetized neutron star ( $B \sim 10^8 - 10^9$  G). However, results of optical spectroscopic and photometric observations suggest that the companion star is a B5–A0 supergiant and has an eccentric binary orbit of  $e = 0.45$  (Jonker et al. 2007). Those properties indicate a HMXB, which usually accompanies a strongly magnetized neutron star ( $B \sim 10^{11} - 10^{12}$  G). The system is really young as Heinz et al. (2013) discovered a young ( $< 4600$  yr) X-ray supernova remnant surrounding Cir X-1. To explain the discrepancy, Heinz et al. (2013)

suggested either that the neutron star magnetic field decayed quickly to below  $10^{12}$  G or that the neutron star was born with such a low field. There was also the same suggestion in Jonker et al. (2007).

The long-term X-ray activity had been continuously monitored with RXTE (Bradt et al. 1993) ASM (All Sky Monitor: Levine et al. 1996) since 1996 to 2011 December. Until 2000, the source had been in a very active phase with a daily average flux of  $\sim 1$  Crab (Parkinson et al. 2003). Since 2000, the activity had declined gradually, and then it reached to the inactive phase with a flux below the detection limit of 10 mCrab and no outburst activity in 2007. In 2009 August, MAXI (Monitor of All-sky X-ray Image: Matsuoka et al. 2009) started the all-sky survey with GSC (Gas Slit Camera: Mihara et al. 2011; Sugizaki et al. 2011) and SSC (Solid-state Slit Camera: Tomida et al. 2011) on the International Space Station. The MAXI nova alert system (Negoro et al. 2010) detected the beginning of an outburst from Cir X-1 on 2010 May 7 (Nakajima et al. 2010). The X-ray flux of the outburst reached  $320 \pm 30$  mCrab on May 8. After the event, the source return to the active phase. D’Aì et al. (2012) analyzed data of RXTE, Swift, and Chandra observations of outbursts from 2010 May 11 to July 4, and reported that the source exhibited a clear spectral transition from an optically thick state (soft state) to an optically thin state (hard state) which can be interpreted within the disk-instability scenario.

In this paper, we report the recent outburst properties of Cir X-1 obtained from MAXI GSC light curve from 2009 August 15 to 2013 December 18. In particular, we investigate the observed behavior of sudden luminosity decrease around the periastron passages. The paper is organized as follows. In section 2, we describe the observations and the light curve analysis, and then estimate the radius of the outer disk. In section 3, we discuss three interpretations for the new sudden luminosity decrease. Finally, we present the conclusions in section 4.

## 2. Observational Data and Analysis

### 2.1. X-ray Light Curves of Outbursts

In this section we examine the behavior of outbursts of Cir X-1 using the light curve data observed by MAXI/GSC<sup>1</sup> and by Swift (Gehrels et al. 2004)/BAT (Burst Alert Telescope: Barthelmy et al. 2005).<sup>2</sup> The comparison of both the data is useful to investigate soft/hard state and propeller effect of neutron star LMXBs similar to Cir X-1 (Asai et al. 2012, 2013). To make easy to compare both data, the count rates of GSC and BAT are converted to luminosities by assuming Crab-like spectrum (Kirsch et al. 2005) and by using a distance of 7.8 kpc employed by D’Aì et al. (2012). Furthermore, because Cir X-1 has a 16.6 d binary period we employ the orbital cycle number as a time scale. The ephemeris is employed from Nicolson (2007) as was in D’Aì et al.

(2012), which is expressed as

$$T_{\text{MJD}}(N) = 43076.32 + (16.57794 \pm 0.00094)N - (0.0000401 \pm 0.0000015)N^2, \quad (1)$$

where  $N$  is the number of 16.6 d cycles since MJD = 43076.32 and refer to the orbital phase calculations based on this ephemeris. Here, we also adopt that the phase 0 corresponds to the periastron because this ephemeris predicts start of most of the X-ray outbursts as mentioned in D’Aì et al. (2012).

Figure 1 shows the one-day averaged GSC light curve in 2–10 keV luminosity against the orbital phase. The light curve starts from MJD = 55058.5 (2009 August 15) until MJD = 56644.5 (2013 December 18). There were 21 outbursts denoted as alphabet (a–u) in the figure. Here we chose remarkable eleven outbursts which continue until the next periastron. These are indicated by alphabets with parentheses in the figure.

These remarkable outbursts are shown in figure 2, as the one-day GSC light curves (2–10 keV), one-day BAT light curves (15–50 keV), and the hardness ratios (BAT/GSC). In the GSC light curve, the detection limit is  $\sim 1 \times 10^{36}$  erg s<sup>-1</sup>. However, the detection limit sometimes increases because of the variability of the background. For example, between outbursts (i) and (j), we cannot recognize the source in the daily GSC image, although the average luminosity was estimated as  $(1.5 \pm 1.0) \times 10^{36}$  erg s<sup>-1</sup>. The spectral state was mostly determined by the BAT(15–50 keV)/GSC(2–10 keV) hardness ratio, where a ratio less than  $\sim 1$  identifies the soft state according to the method employed in Asai et al. (2012). However, when the data points for the GSC and/or BAT have large errors, it is difficult to distinguish the states. In this case, we judged the state using the luminosity of the spectral state transition of the outburst (b) reported by D’Aì et al. (2012), that is,  $(3.5 \pm 0.7) \times 10^{36}$  erg s<sup>-1</sup>. Thus obtained periods of the soft state are denoted in figure 2.

We note the following four points from figures 1 and 2 :

- (1) The seven outbursts, (i), (j), (l), (m), (p), (s), and (u), reveal sudden luminosity decrease around the periastron, and then the outbursts terminated. Such decreasing feature has not been detected in any outburst of LMXBs embedding weakly magnetized neutron star. This feature is a main subject to be investigated in this paper.
- (2) There are three outbursts (i), (s), and (t), which show very soft state (BAT/GSC  $\sim 0.01$ ). Their peak luminosities in the 2–10 keV band (GSC) are very high,  $\gtrsim 1.5 \times 10^{38}$  erg s<sup>-1</sup>, which is almost the Eddington luminosity. On the other hand, the luminosities in the 15–50 keV band (BAT) are very low ( $\lesssim 1 \times 10^{36}$  erg s<sup>-1</sup>). This means that the blackbody emission increases without Comptonized emission at the onset. This very soft state would be another disk state, such as a slim disk, which is sometimes observed in Z sources (e.g., Lin et al. 2012).
- (3) At the peak of outburst k, the BAT/GSC hardness ra-

2229: 2231: <sup>1</sup> <<http://maxi.riken.jp/>>.

2229: 2231: <sup>2</sup> <<http://heasarc.gsfc.nasa.gov/docs/swift/results/transients/>>.

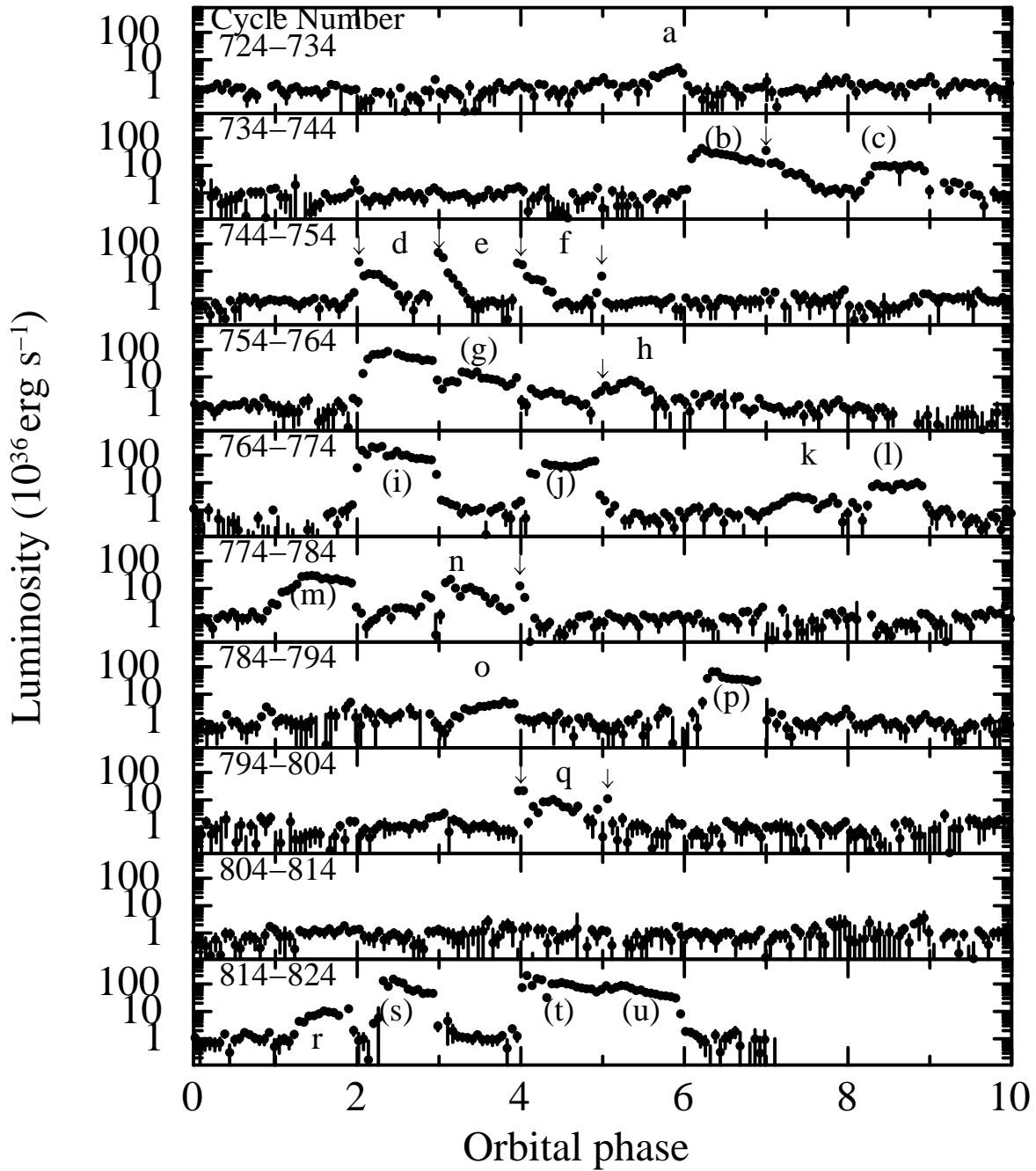


**Fig. 1.** Light curve in 2-10 keV luminosity ( $d=7.8$  kpc) against orbital phase. The data are one-day averaged. The alphabets (a–u) denote the outbursts observed. The alphabets with parentheses denote that the outbursts continue until next periastron. Arrows indicate the data points of “periastron spike” (see the text).

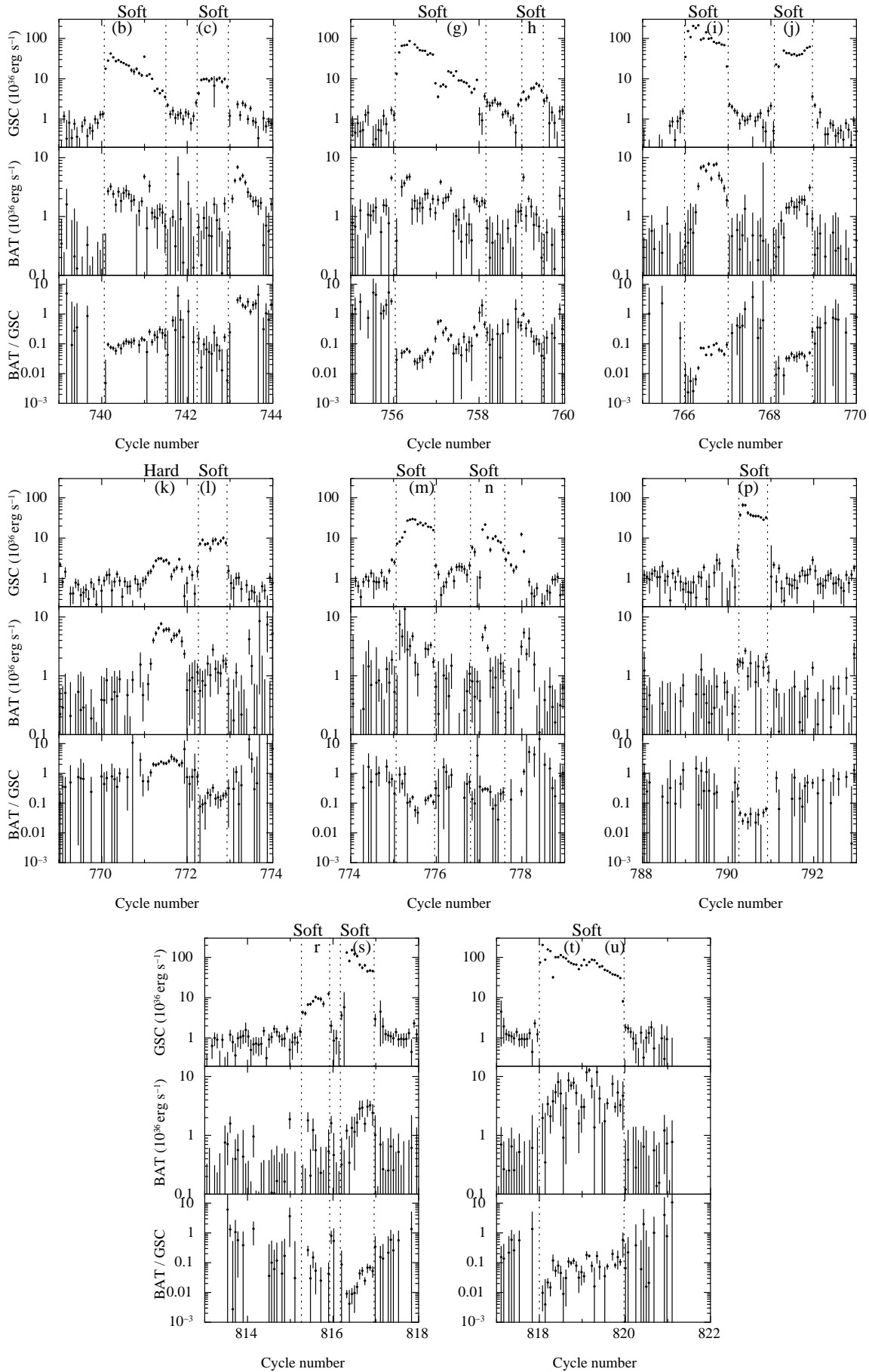


**Fig. 2.** One-day GSC light curves (2–10 keV), one-day BAT light curves (15–50 keV), and the hardness ratios (BAT/GSC) for the outburst periods remarked in figure 1. The region between two vertical dotted lines indicates the soft state as noted above the figure. The vertical error bars represent 1- $\sigma$  statistical uncertainty.

**Table 1.** Periastron spike.

Cycle Number*	Peak phase	Peak Luminosity <sup>†</sup>	Location to an outburst
741	0.0023	$49 \pm 3$	during outburst (b)
746	-0.0071	$93 \pm 4$	onset of outburst d
747	-0.0005	$161 \pm 6$	onset of outburst e
748	-0.0130	$173 \pm 7$	onset of outburst f
749	-0.0330	$21 \pm 2$	no outburst
759	0.0170	$12 \pm 2$	during outburst h
778	0.0171	$24 \pm 3$	end of outburst n
798	0.0031	$250 \pm 10$	onset of outburst q
799	0.0363	$17 \pm 3$	end of outburst q

\* Orbital cycle number defined by Nicolson (2007).

† Luminosity in unit of  $10^{36}$  erg  $s^{-1}$  in 2–10 keV energy band. The errors are in  $1-\sigma$ .

tio remained above 1. This indicates the hard state throughout the outburst. Although the peak of the other outbursts is usually in the soft state, this is only one exception in our observation (see figure 2). The peak luminosity of this outburst in 2–10 keV was low ( $\sim 3 \times 10^{36}$  erg  $s^{-1}$ ), whereas that in 15–50 keV was high (i.e., a “hard outburst”).

- (4) Jumps (burst-like points) appeared between phases  $-0.05$  and  $0.05$  at nine periastron passages, indicated by arrows in figure 1. The luminosities are above  $1 \times 10^{37}$  erg  $s^{-1}$  and they occurred independently of the outbursts. We call them “periastron spikes.” The properties of the nine periastron spikes are summarized in table 1. Here, we used the data of each scan, which is usually performed once during the 92 min orbital period of MAXI. The detailed analysis revealed that the hardness ratio of 4–10 keV to 2–4 keV did not show any softening, as an example is shown in figure 3. Thus, the periastron spikes are not type-I X-ray bursts. It would be caused by a temporary increase of the accretion rate independent of the existence of the accretion disk, such as spherical accretion from the polar directions. Further discussion on this spike will be made in subsection 3.3

## 2.2. Variation around Periastron Passage

The properties of 21 outbursts (a–u) are summarized in table 2. As shown in the table, the outbursts start in an orbital phase between  $\sim -0.3$  and  $\sim 0.2$ , except outburst a. Eleven outbursts (alphabets with parentheses in figure 1 and 2, and remarkable outbursts in subsection 2.1) continued to the next periastron. The behavior at the next periastron can be classified into three types: “continuous outburst” [i.e., (b), (c), and (g)], “sudden drop” [i.e., (i), (j), (l), (m), (p), (s), and (u)], “next new outburst” [i.e., (t)], which are denoted in table 2. The features of three types are summarized as below:

**Continuous outbursts:** Outbursts (b), (c), and (g) continued smoothly to the next orbital cycle after

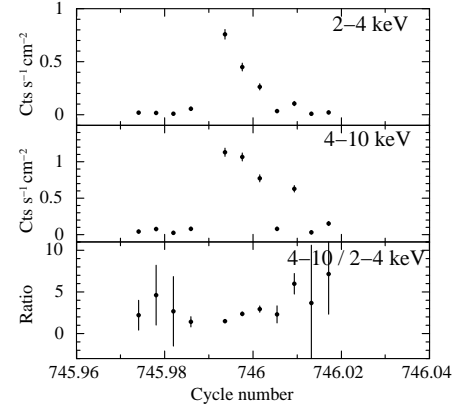


**Fig. 3.** GSC light curves and hardness ratio of periastron spike at cycle number = 746. The time of the spike is MJD = 55421.0432. Data points are of each scan. Decay of flux is seen over several scans in this spike. The vertical error bars represent  $1-\sigma$  statistical uncertainty.

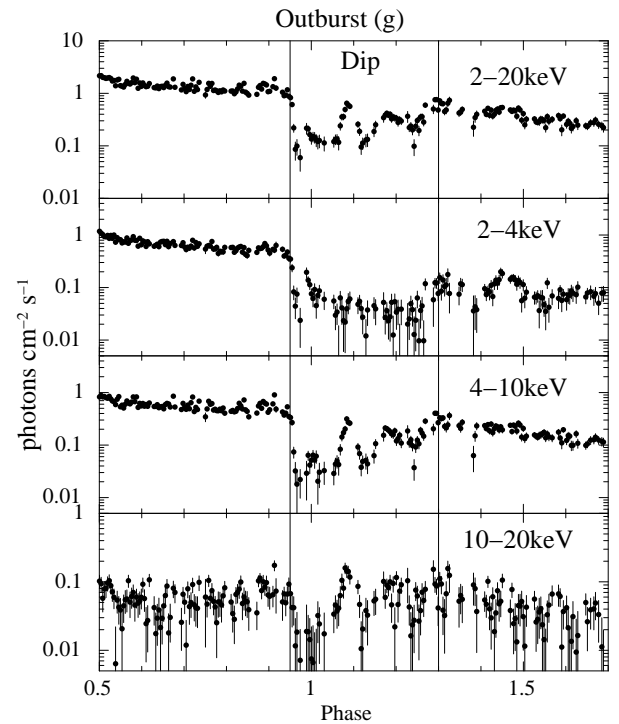


**Fig. 4.** One-orbit (92-min) averages GSC light curves of outburst (g) in four energy bands around the next periastron passage (phase 1 is  $N = 757$ ). The dip was seen from phase  $\sim 0.95$  to  $\sim 1.3$ , which are shown by the region between two vertical lines. The vertical error bars represent  $1-\sigma$  statistical uncertainty.

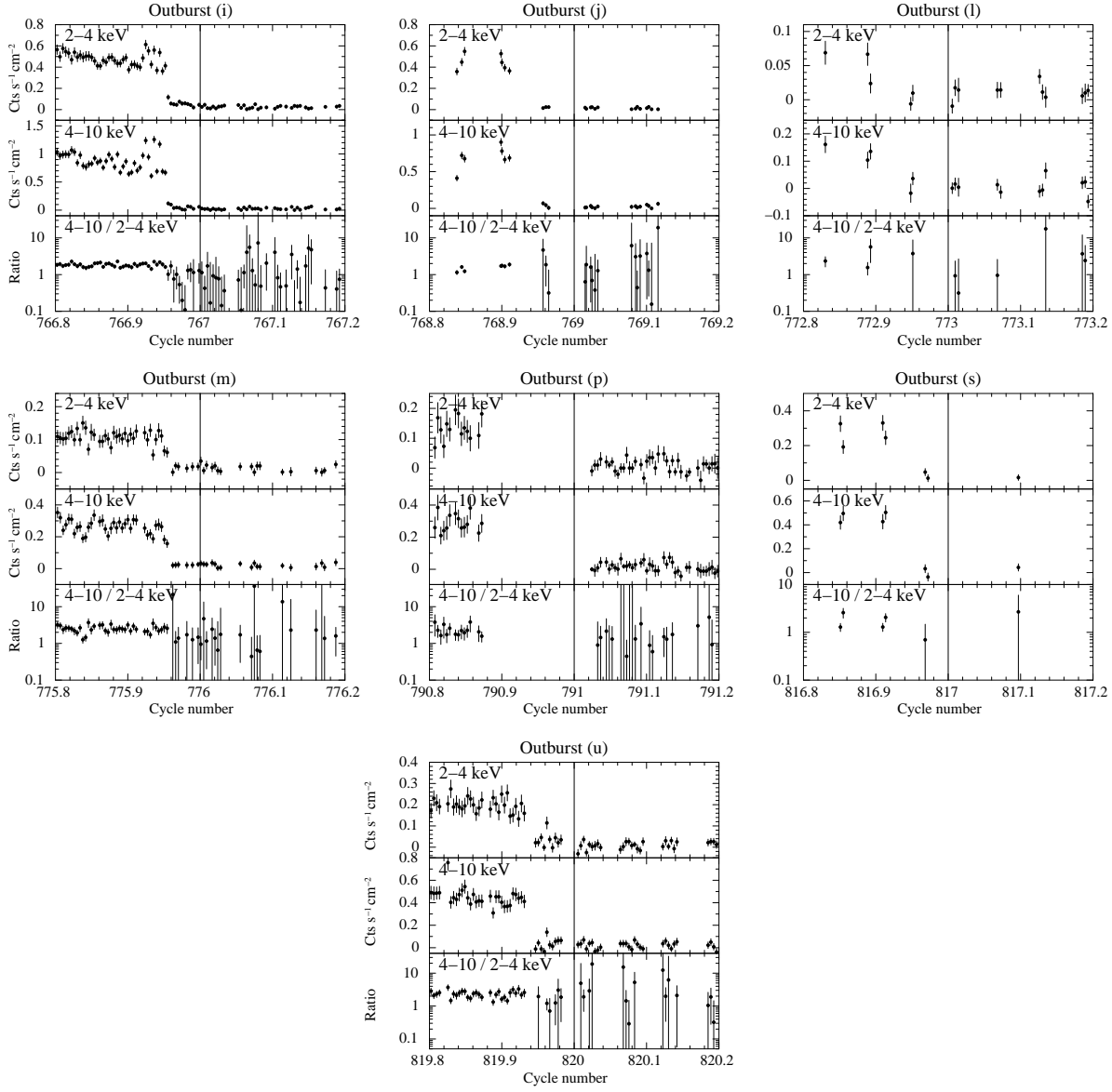


**Fig. 5.** Magnified GSC light curves of outbursts and hardness ratios around periastron passage for seven outbursts classified as “sudden drop” in subsection 2.2. The vertical line indicate a phase of periastron. Data points are of each scan. The vertical error bars represent  $1-\sigma$  statistical uncertainty. In outburst (p), there is a large data gap around the periastron (cycle number 791)

**Table 2.** Outbursts observed by MAXI/GSC.

Outburst*	Onset <sup>†</sup> (phase)	Peak day <sup>‡</sup> (MJD)	Peak luminosity <sup>§</sup>	State at peak	Behaviour around periastron <sup>l</sup>	Luminosity <sup>§</sup> before sudden drop	Luminosity <sup>§</sup> after sudden drop
a	$-0.41 \pm 0.03$	55155.5	$5.1 \pm 0.3$	soft	not clear	–	–
(b)	$0.06 \pm 0.03$	55325.5	$42.4 \pm 0.9$	soft	continuous	$(12 \pm 1)^{\#}$	–
(c)	$0.18 \pm 0.03$	55362.5	$9.9 \pm 0.6$	soft	continuous	$(6.3 \pm 0.7)^{\#}$	–
d	$-0.07 \pm 0.03$	55423.5	$8.1 \pm 0.3$	soft	–	–	–
e	$-0.07 \pm 0.06$	55439.5	$8.7 \pm 0.7$	soft	–	–	–
f	$-0.07 \pm 0.03$	55455.5	$6.5 \pm 0.3$	soft	–	–	–
(g)	$0.04 \pm 0.03$	55592.5	$86 \pm 2$	soft	continuous	$(39.9 \pm 0.7)^{\#}$	–
h	$-0.12 \pm 0.03$	55641.5	$7.6 \pm 0.6$	soft	–	–	–
(i)	$-0.03 \pm 0.03$	55752.5	$153 \pm 2$	soft	sudden drop	$68.4 \pm 0.8$	$1.5 \pm 1.0$
(j)	$0.08 \pm 0.03$	55799.5	$62 \pm 2$	soft	sudden drop	$62 \pm 2$	$< 1.6$
k	$0.05 \pm 0.03$	55840.5	$3.1 \pm 0.2$	hard	–	–	–
(l)	$0.20 \pm 0.03$	55864.5	$10.1 \pm 0.8$	soft	sudden drop	$7.6 \pm 0.8$	$< 2$
(m)	$-0.14 \pm 0.03$	55907.5	$29.8 \pm 0.6$	soft	sudden drop	$15.8 \pm 0.4$	$1.5 \pm 1.0$
n	$-0.26 \pm 0.03$	55935.5	$22 \pm 1$	soft	–	–	–
o	$0.15 \pm 0.03$	56111.5	$5.5 \pm 0.5$	soft	not clear	–	–
(p)	$0.18 \pm 0.03$	56153.5	$66 \pm 6$	soft	sudden drop	$32 \pm 2$	$1.7 \pm 1.5$
q	$-0.01 \pm 0.09$	56286.5	$10 \pm 1$	soft	–	–	–
r	$0.24 \pm 0.03$	56575.5	$13 \pm 1$	soft	–	–	–
(s)	$0.12 \pm 0.06$	56584.5	$152 \pm 10$	soft	sudden drop	$46 \pm 3$	$1.7 \pm 1.4$
(t)	$-0.05 \pm 0.03$	56611.5	$203 \pm 3$	soft	next outburst	$(62 \pm 2)^{\#}$	–
(u)	$-0.07 \pm 0.03$	56630.5	$88 \pm 1$	soft	sudden drop	$30.6 \pm 0.9$	$1.5 \pm 1.3$

\* The alphabets with parentheses denote that the outbursts continue until next periastron.

<sup>†</sup> In order to define the “onset phase”, we defined “last off state” and “first on state”. The “last off state” indicates the lowest data point, after which the flux increased monotonically towards the peak of the outburst. The “first on state” indicates the first data point which has a significantly higher flux than that of the “last off state”. The “onset phase” is defined by the middle of the “last off state” and the “first on state”, and the error is defined by the span between the both data points.

<sup>‡</sup> Day of maximum luminosity in the 2–10 keV GSC light curve in one day bin.

<sup>§</sup> Luminosity in unit of  $10^{36}$  erg  $s^{-1}$  in 2–10 keV energy band. The errors are 1- $\sigma$  errors.

<sup>l</sup> The X-ray behaviour around periastron passage. “sudden drop” denotes that the luminosity suddenly decreases around periastron passage and the outburst seems to have ended. “continuous” (continuous outburst) denotes that the outburst continues after periastron passage. “next outburst” (next new outburst) denotes that next outburst seems to start after periastron passage. “not clear” denotes that the distinction of “sudden drop” and “dip” is not clear, because of low peak luminosity. “–” denotes that the outburst had ended before next periastron passage.

<sup>#</sup> Luminosity at phase  $\sim 0.95$  before next dip.

periastron passage, although the intensity decreased temporarily around periastron. The intensity decreases are interpreted as the absorption dip that was often observed before an outburst onset when the luminosity was high in 1996–2000 (Clarkson et al. 2004). In particular, the outburst (g) shows a clear absorption dip, which can be understood from the light curves divided in energy band. In figure 4, we show the light curves of outburst (g) in four energy bands, 2–20 keV, 2–4 keV, 4–10 keV, and 10–20 keV, using one-orbit (92-min) averaged data. The energy dependence of the light curves shows that the dip is caused by a cold absorber. The dip continued from phase  $\sim 0.95$  to  $\sim 1.3$ . In outbursts (b) and (c), the dip is not clear in the GSC light curve. However, D’Ài et al. (2012) reported that the spectral shape was affected by the variable cold absorber. They obtained the absorption values of  $N_{\text{H}} \sim 5 \times 10^{22}$   $\text{cm}^{-2}$  and  $N_{\text{H}} \sim 6 \times 10^{23}$   $\text{cm}^{-2}$  for outburst (b) (around cycle number 741) using RXTE data and outburst

(c) (around cycle number 743) using Swift data, respectively.

D’Ài et al. (2012) also reported that the outburst (c) seems to turn off suddenly near periastron passage (cycle number 743) in the ASM light curve. In the GSC light curve (figure 2), the outburst seems to continue with a gradual decrease, although there is a large data gap. The BAT light curve shows a sudden increase just after periastron passage, which is like a hard outburst. In the present data, we cannot distinguish either whether outburst (c) ended and another hard outburst started, or whether the state changed to a hard state during outburst (c).

**Next new outburst:** Outburst (t) also appears to continue to the next orbital cycle after periastron passage. However, the decay profile does not continue to that after dip (see figure 6 in subsection 2.3). A new outburst seems to occur at the next periastron during the soft state. This behavior resembles that of the outbursts caused by the enhanced mass trans-

fer when the luminosity was high in 1996–2000 (e.g., Clarkson et al. 2004). We classified outburst (t) as the “next new outburst”.

**Sudden drop:** In contrast to the continuous outburst and the next new outburst, outbursts (i), (j), (l), (m), (p), (s), and (u) show a sudden luminosity decrease around periastron. The seven outbursts were also described in subsection 2.1 (1). In order to examine the detailed variability around the sudden decrease phase, we plotted their detailed GSC light curves and GSC hardness ratios (4–10 / 2–4 keV) using the short time scale data of each scan (92 min) as shown in figure 5. The sudden decrease at phase  $\sim 0.95$  is seen clearly in (i), (m), and (u), in which the time scale is about 90 min. The sudden luminosity decreases of other outbursts (j), (l), (p), and (s) are consistent with the occurrence at a phase around 0.95 although there are considerable data gaps.

The sudden luminosity decreases at phase  $\sim 0.95$  resembles the dip of outburst (g) in the point of the time-scale of a few hours. However, in these seven outbursts, the luminosities after the sudden drop remained low in hard state until the next outburst. The luminosities before and after the sudden drop are summarized in table 2. The luminosity range just before the sudden drop is  $(6\text{--}70) \times 10^{36} \text{ erg s}^{-1}$ , and the spectral state is in soft state judging from the hardness ratio (BAT/GSC) in figure 2. These results are consistent with the report of D’Aì et al. (2012) that the luminosity of the spectral state transition occurs at  $(3.5 \pm 0.7) \times 10^{36} \text{ erg s}^{-1}$ . After the sudden drop, the luminosities stay below  $\sim 3 \times 10^{36} \text{ erg s}^{-1}$ . Although the spectral state is not clear from the hardness ratio (BAT/GSC) in figure 2 because of large uncertainties, the low luminosities indicate that it is most likely the hard state (D’Aì et al. 2012). We discuss the possible cause of the sudden drop in the next section.

Here, it is noted that there is an interesting information on radio observations for outburst (m) although radio observations for others are not reported. Namely, large radio flares were observed after the periastron passages of the end of outburst (m) (cycle number = 776) and the beginning of outburst n (cycle number = 777) (Armstrong et al. 2013).

### 2.3. Estimate of Outer Radius from Outburst Decay Curve

In the MAXI Cir X-1 observations, the persistent luminosity was low and the source sometimes caused an X-ray outburst. This behavior reminds us of soft X-ray transients (Campana et al. 1998a). Their recurrent outburst behavior is usually interpreted by the thermal viscous disk instability model (DIM: Lasota 2001). D’Aì et al. (2012) reported to have analyzed outburst (b) that the source showed a clear spectral state transition, from an optically thick state (soft state) to an optically thin

state (hard state) and that this is interpreted it via the DIM. Therefore, we also analyze the light curves of the outbursts on the basis of the DIM.

The morphology of the outbursts is generally characterized by the fast rise exponential decay (FRED) behavior, and the DIM is essentially able to explain it. However, the DIM alone cannot reproduce a realistic FRED outburst. The X-ray irradiation effect is considered to be very important. If the edge of the outer disk is sufficiently ionized by irradiation, outburst exponentially decays (King & Ritter 1998). In contrast, if the disk irradiation is not strong enough, the edge of the outer disk is neutral and linear decay is expected. This also means that the exponential decay may change to the linear decay when the X-ray luminosity decreases sufficiently during the decay phase. Powell, Haswell, and Falanga (2007) labeled this change in the light curve as a “brink.” In this subsection, we estimate the outer radius of the accretion disk by using the fitting results of the linear and exponential function under the DIM model. In this estimation, we used the one-orbit (92-min) average GSC light curve for the fitting.

In order to estimate the outer radius, we chose nine outbursts with clear decay profiles in the 2–10 keV band [(b), (g), (i), (j), (m), (p), (s), (t), and (u)] from the remarkable eleven outbursts (in subsection 2.1). Here we removed (c) and (l), as they showed a flat-top profile. First, we fitted the decay part by a linear function as

$$L(\varphi) = -\gamma \times \varphi + C, \quad (2)$$

where  $\varphi$  is the orbital phase,  $\gamma$  is the slope, and  $C$  is the luminosity at  $\varphi = 0$ . Here,  $\varphi = 1$  is the next periastron after outburst onset. The sudden drop occurs at  $\varphi = 0.95$ . The fitting results are summarized in table 3 and indicated by dashed lines in figure 6.

Next, we fitted each outburst by an exponential-decay function. The X-ray luminosity is given by

$$L(\varphi) = L_S \exp[-(\varphi - \varphi_S)/\tau], \quad (3)$$

where  $\varphi_S$  is the phase at the beginning of the fitting, which was fixed.  $L_S$  is the luminosity at  $\varphi_S$ , and  $\tau$  is the time-scale of the decay. The fitting results are summarized in table 3 and indicated by dash-dotted lines in figure 6.

For outburst (b), D’Aì et al. (2012) reported that the light curve is described well by a combination of two linear decays with the 2–60 keV RXTE light curve for  $\varphi = 0.3\text{--}1.68$ . On the other hand, the GSC light curve in 2–10 keV can be fitted by either a single linear decay or a single exponential decay with the same reduced  $\chi^2$ . The difference may be caused by the difference in intervals and sampling frequency between the pointing observations with RXTE and the monitoring observations with MAXI.

The outer disk radius  $R_{\text{outer}}$  can be estimated independently using either the brink luminosity and the slope of linear decay (hereafter brink model) or the time-scale of the exponential decay (Powell et al. 2007; Campana et al. 2013). In the brink model, using the slope of the linear decay  $\gamma$  and the brink luminosity  $L_{\text{brink}}$ ,  $R_{\text{outer}}$  can be derived as

$$R_{\text{outer}} = (3 \nu_{\text{KR}} L_{\text{brink}} / \gamma)^{1/2}, \quad (4)$$



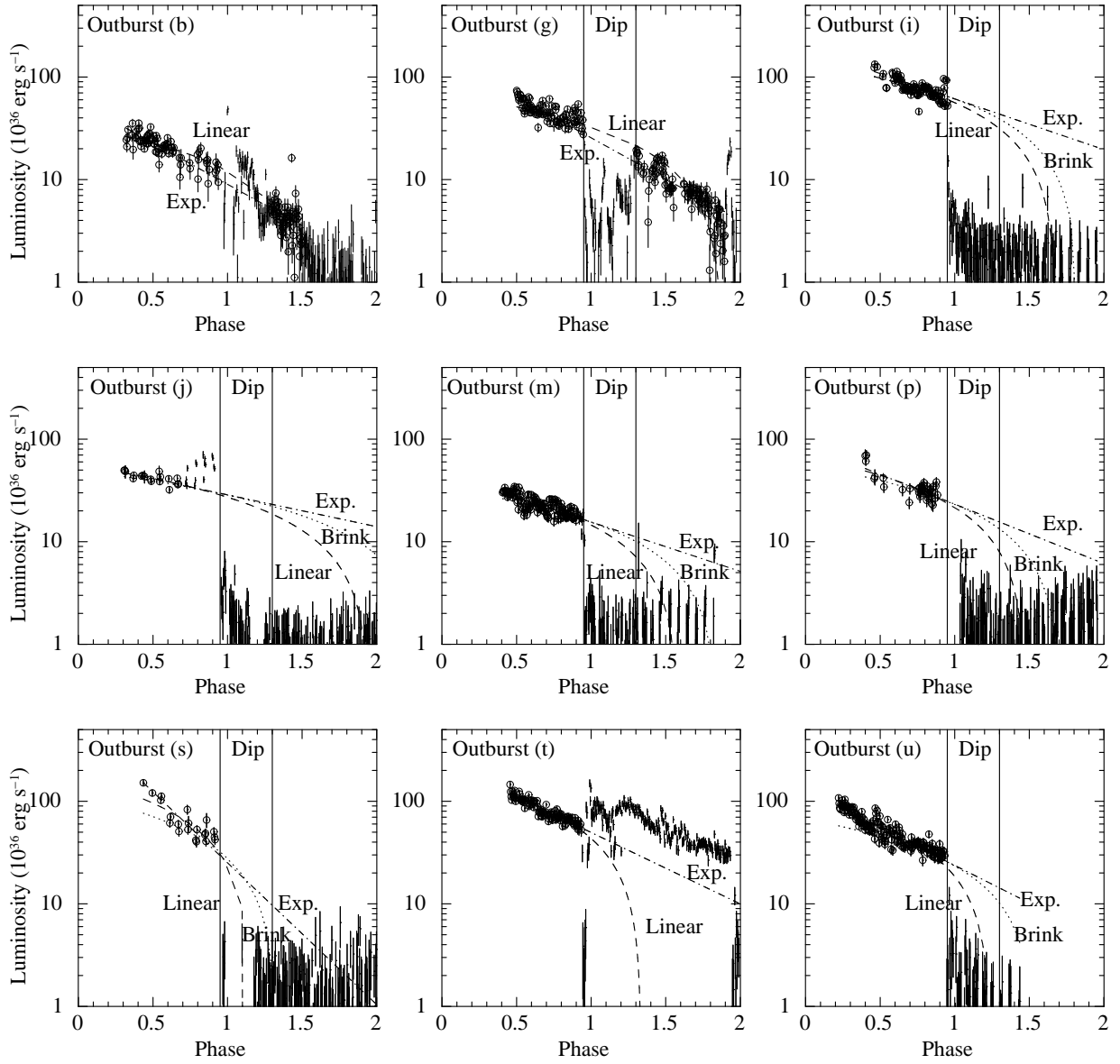


**Fig. 6.** One-orbit (92-min) averages GSC light curves in 2-10 keV energy band and fitting results. The dashed lines show the best-fit linear decay and the dash-dotted lines show the best-fit exponential decay. Parameters are listed in table 3. The dotted lines show the linear decay expected by brink model. The region between two vertical lines is when there is a possibility of dip.

**Table 3.** Parameters of linear and exponential decay fits of outbursts.

Outburst	Interval *	Linear decay fit				Exponential decay fit			
		$\gamma^\dagger$	$C^\ddagger$	$R_{\text{outer}}^\S$	$\chi^2$ (dof)	$L_S^l$	$\tau^\#$	$R_{\text{outer}}^{**}$	$\chi^2$ (dof)
(b)	0.30–1.5 <sup>††</sup>	$20.8^{+0.5}_{-0.4}$	$33.1 \pm 0.6$	$> 7.5$	2.8 (133)	$32.9 \pm 0.8$	$0.54^{+0.02}_{-0.01}$	$4.82^{+0.09}_{-0.04}$	2.8 (132)
(g)	0.30–1.9 <sup>††</sup>	$37.2^{+0.4}_{-0.5}$	$70 \pm 1$	$> 7.7$	7.5 (202)	$64.5^{+0.7}_{-0.8}$	$0.54^{+0.01}_{-0.01}$	$4.82 \pm 0.04$	5.3 (201)
(i)	0.46–0.95	$83 \pm 6$	$139 \pm 5$	$> 7.2$	7.1 (98)	$113 \pm 3$	$0.88^{+0.06}_{-0.06}$	$6.2^{+0.2}_{-0.3}$	6.9 (97)
(j)	0.30–0.68	$29^{+9}_{-10}$	$56 \pm 5$	$> 8.4$	1.1 (18)	$47^{+3}_{-2}$	$1.4^{+0.7}_{-0.3}$	$8^{+2}_{-1}$	1.1 (17)
(m)	0.40–0.90	$25 \pm 2$	$39^{+2}_{-1}$	$> 7.0$	2.5 (125)	$30.0^{+0.7}_{-1.0}$	$0.90^{+0.08}_{-0.06}$	$6.2^{+0.3}_{-0.2}$	2.5 (124)
(p)	0.35–0.88	$46^{+8}_{-9}$	$67^{+7}_{-6}$	$> 6.9$	2.1 (38)	$55.5^{+4.8}_{-4.6}$	$0.75^{+0.14}_{-0.10}$	$5.7^{+0.5}_{-0.4}$	1.87 (37)
(s)	0.44–0.92	$145^{+17}_{-34}$	$160^{+21}_{-5}$	$> 5.4$	5.5 (21)	$129^{+10}_{-9}$	$0.37^{+0.05}_{-0.03}$	$4.0^{+0.3}_{-0.2}$	4.01 (20)
(t)	0.46–0.93	$130 \pm 6$	$173 \pm 4$	$> 6.1$	2.6 (106)	$119 \pm 2$	$0.62^{+0.03}_{-0.02}$	$5.2 \pm 0.1$	2.28 (105)
(u)	0.22–0.93	$77^{+3}_{-1}$	$96 \pm 2$	$> 6.6$	4.2 (171)	$88 \pm 2$	$0.59^{+0.02}_{-0.02}$	$5.0 \pm 0.1$	3.07 (170)

\* Phase interval used for model fits.

<sup>†</sup> Slope of linear decay in units of  $10^{36}$  erg  $\text{s}^{-1}$  phase $^{-1}$ .

<sup>‡</sup> Luminosity at phase 0 in units of  $10^{36}$  erg  $\text{s}^{-1}$ .

<sup>§</sup> Outer radius in units of  $10^{10}$  cm of the accretion disk estimated by the brink model, assuming that the brink occurred at or before the beginning of the decay phase.

<sup>l</sup> Luminosity at the beginning of the interval in units of  $10^{36}$  erg  $\text{s}^{-1}$ .

<sup>#</sup> Time constant of exponential decay in units of orbital period.

\*\* Outer radius in units of  $10^{10}$  cm of the accretion disk estimated from the time constant of exponential decay.

<sup>††</sup> Except for the phase of 0.95–1.3 to avoid dips.

where  $\nu_{\text{KR}}$  is the viscosity at the edge of the outer disk. King and Ritter (1998) adopted  $\nu_{\text{KR}} \sim 10^{15}$  cm $^2$  s $^{-1}$ . However, the brink feature was not recognized in all the outbursts. Applying the brink model, we can assume that the brink occurred at the beginning of the decay phase or had already occurred earlier. Then the luminosity at the decay start  $L_{\text{start}}$  (at the phase corresponding to the first value of the interval in table 3) is taken as the lower limit of the brink luminosity. Then we can estimate the lower limit of  $R_{\text{outer}}$  as

$$R_{\text{outer}} > (3 \nu_{\text{KR}} L_{\text{start}} / \gamma)^{1/2}. \quad (5)$$

The estimated outer disk radii are summarized in table 3.

On the other hand, in the exponential decay model, the outer disk radius is given by the time-scale  $\tau$  of the exponential decay as

$$R_{\text{outer}} = (3 \nu_{\text{KR}} \tau)^{1/2}. \quad (6)$$

The estimated outer disk radii are summarized in table 3. The outer radii in the outbursts are estimated as  $\sim 5 \times 10^{10}$  cm assuming the exponential decay. Here, we examined the relationship between the estimated outer radius assuming exponential decay and the peak luminosity or the luminosity just before the sudden drop around phase  $\varphi = 0.95$ . There is no correlation between these luminosities and the outer radius.

### 3. Discussion

We found sudden luminosity decreases around periastron in 7 out of 21 outbursts observed with MAXI/GSC. The luminosities dropped from a few times  $10^{37}$  erg  $\text{s}^{-1}$  to  $\lesssim 3 \times 10^{36}$  erg  $\text{s}^{-1}$ , and this was followed by inactive states lasting for 14–16 d. The light curve of the decay part can be fitted as well by either a single linear func-

tion or a single exponential function. In this section, we propose three interpretations for the sudden luminosity decrease: the end of the outburst during the dip, the propeller effect, and the stripping effect by the stellar wind of the companion star.

#### 3.1. End of outburst during dip

The sudden luminosity decrease in the seven outbursts, (i), (j), (l), (m), (p), (s), and (u), always occurred during periastron passage. In Cir X-1, a dip was often observed during periastron passage. Therefore, we consider that the luminosity became sufficiently low after the dip, and the outburst seems to have ended. The dip was assumed to continue from phase  $\sim 0.95$  to  $\sim 1.3$  as observed in outburst (g) (see figure 4). The decay profile during the dip was assumed to be three cases: exponential decay, linear decay, and brink model. In the case of exponential decay and linear decay, we extrapolated the fitting results for the decay profile in subsection 2.3, and plotted them in figure 6. The brink model assumes that the brink occurred during the dip, where the decay profile changed from exponential to linear. The slope  $\gamma$  of the brink model can be limited by equation (4). In order to obtain the fastest decay case in the brink model, the brink was assumed to occur at phase 0.95. The  $L_{\text{brink}}$  values at phase 0.95 were obtained by the exponential-decay fit. The outer radius  $R_{\text{outer}}$  was calculated by the exponential-decay fit as well. Thus, we obtained the slope  $\gamma$  of the brink model. In figure 6, the dotted lines show the linear decay expected from the brink model. Here, the outburst (l) is excluded since none of the exponential and linear fittings worked for its flat-top profile (see subsection 2.3).

As shown in figure 6, the observed data points after the drop lie far below the three fitted lines except for outbursts (s) and (u). This implies that it is difficult to explain

the sudden drop in terms of the interpretation that the outburst ended during the dip. For outbursts (s) and (u), it is possible to explain the sudden drop by a combination of the dip of phase 0.95–1.3 and rapid linear decay, i.e., with linear decay or a brink in outburst (s), and linear decay in outburst (u).

### 3.2. Propeller Effect

Sudden luminosity decrease is often attributed to the propeller effect (Campana et al. 1998b, 2008; Matsuoka & Asai 2013; Asai et al. 2013). The propeller luminosity is related to the magnetic field and spin period of the neutron star as (Matsuoka & Asai 2013)

$$L = 1.5 \times 10^{37} \eta^{-7/2} P_1^{-7/3} B_8^2 \text{ erg s}^{-1}, \quad (7)$$

where  $P_1$  is the spin period of the neutron star in ms, and  $B_8$  is the magnetic field of the neutron star in units of  $10^8$  G. The values  $(P_1, B_8)$  are specific to the system, but they are not known for Cir X-1. Here  $\eta \sim 0.5\text{--}1$  is a factor representing the geometry of the accretion flow; it was introduced in the definition of the Alfvén radius as  $R_A = \eta R_{A0}$ , where  $R_{A0}$  is the ideal Alfvén radius in equation (27) in Ghosh and Lamb (1979). The  $\eta$  also appears in Burderi et al. (1998) as  $\phi$ . Approximately,  $\eta \sim 0.5$  corresponds to a disk-like accretion flow and  $\eta \sim 1$  corresponds to a spherical accretion flow. Thus, the propeller luminosity depends on the geometry of the accretion flow as  $L \sim 1.3 \times 10^{36} P_1^{-7/3} B_8^2 \text{ erg s}^{-1}$  if it is disk-like, and  $L \sim 1.5 \times 10^{37} P_1^{-7/3} B_8^2 \text{ erg s}^{-1}$  if it is spherical. Here, we notice that Wang (1997) estimated the  $\eta$  ( $\phi$  in Burderi et al. 1998)  $\sim 1$  even in the case of disk-like accretion flow. They calculated torque in inclined magnetic moment axis to the spin axis assuming that the spin axis is normal to the disk plane. However, we use  $\eta \sim 0.5\text{--}1$  as was used traditionally.

The soft state is usually considered to be a manifestation of an optically thick disk accretion. The spectral states before the sudden drop are soft states in all seven outbursts, judging from the hardness ratio (BAT/GSC) in figure 2. D’Ài et al. (2012) reported that a soft-to-hard state transition occurred at a luminosity of  $(3.5 \pm 0.7) \times 10^{36} \text{ erg s}^{-1}$  in the decay part of outburst (b). This is within the commonly reported transition luminosity in the decay phase, which is 1%–4% of the Eddington luminosity (Maccarone 2003). In outbursts (b) and (g) in figure 2, the spectral state remained in the soft state above this luminosity, which is consistent with D’Ài et al. (2012). This means there was no sudden drop in the soft-state period, which indicates that the propeller effect did not occur above this luminosity. Therefore, it is difficult to explain the sudden drop in terms of the propeller effect.

Here we notice that the state-transition may be still possible at high luminosity in the truncated disk model of Gierliński et al. (2008). If the inner disk is truncated at some point as the outburst decays, the disk may recede. Then, the disk-state may transit from the soft state to the hard state even at a luminosity higher than the usual transition luminosity. Then, the accretion flow may

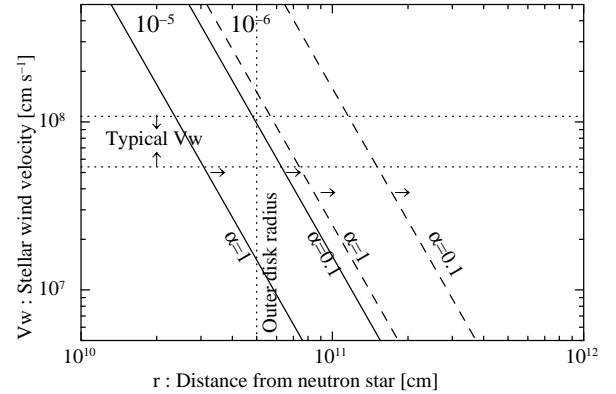


**Fig. 7.** Allowed regions in a plane of stellar wind velocity and distance from the neutron star. Typical stellar wind velocity is between the horizontal dotted lines. The vertical dotted line indicates estimated typical outer radius assuming the exponential decay (see text). The right side of solid and dashed lines are the region which fulfills the condition of wind stripping. The left solid lines are  $\dot{M}_c = 10^{-5} M_\odot \text{yr}^{-1}$  and the right dashed lines are  $\dot{M}_c = 10^{-6} M_\odot \text{yr}^{-1}$ . A set of two lines indicate when  $\alpha = 1$  and 0.1.

change from disk-like to spherical and the propeller effect may occur during the dip, because the propeller luminosity depends on the geometry of the accretion flow. A careful examination of the behavior before the sudden drop at phase  $\sim 0.95$  in outbursts (i) and (j) (see figure 5 and 6) reveals that the luminosity is quite variable, which might suggest an unstable inner disk.

### 3.3. Wind Stripping

A sudden drop can occur around periastron, where the stellar wind of the companion star interacts strongly with the accretion disk around the neutron star (Johnston et al. 1999). If the stellar wind strips a large part of the accretion disk, the disk may cause the state transition in the outer part. As a result, mass accretion rate may decrease rapidly.

We examine the possibility of wind stripping. The condition for wind stripping is that the ram pressure of the stellar wind ( $\rho_w V_w^2$ ) is larger than the gas pressure of the accretion disk ( $P_g$ ). Here, assuming a spherical stellar wind, the density of the stellar wind is given by

$$\rho_w = \dot{M}_c / (V_w 4\pi d^2), \quad (8)$$

where  $\dot{M}_c$  is the mass loss rate of the companion star, and  $d$  is the distance from the center of the companion star. The gas pressure of the accretion disk on the equatorial plane is

$$P_g = G M_{\text{NS}} r^{-3} H^2 \rho_d, \quad (9)$$

where  $M_{\text{NS}}$  is the mass of the neutron star,  $H$  is the half-thickness of the disk, and  $\rho_d$  is the density on the equatorial plane of the outer accretion disk. The density,  $\rho_d$ , is given by Kato et al. (1998) as

$$\rho_d = 37 \alpha^{-7/10} M_{1.4}^{-7/10} (L_X/L_E)^{11/20} \times (r/r_g)^{-15/8} f^{11/20} \text{ g cm}^{-3}, \quad (10)$$

where  $\alpha$  is the viscosity parameter,  $M_{1.4}$  is the neutron star mass normalized by  $1.4M_{\odot}$ ,  $L_X$  is the X-ray luminosity,  $L_E$  is the Eddington luminosity ( $L_E \sim 2 \times 10^{38}$  erg s $^{-1}$ ),  $r$  is the distance from the neutron star,  $r_g$  is the Schwarzschild radius of the neutron star, and  $f = 1 - (r_{\text{in}}/r)^{1/2}$  (where  $r_{\text{in}}$  is the inner disk radius). The half thickness of the disk,  $H$ , is also given by Kato et al. (1998) as

$$H = 2.0 \times 10^3 \alpha^{-1/10} M_{1.4}^{9/10} (L_X/L_E)^{3/20} \times (r/r_g)^{9/8} f^{3/20} \text{ cm.} \quad (11)$$

Figure 7 shows the allowed regions in the plane of the stellar wind velocity and distance from the neutron star. In this calculation, we adopted  $\dot{M}_c = 10^{-5}M_{\odot}\text{yr}^{-1}$  and  $10^{-6}M_{\odot}\text{yr}^{-1}$ . The value of  $d = 2.4 \times 10^{12}$  cm at periastron was calculated using the third Kepler law and the values, eccentricity = 0.45,  $M_c = 10M_{\odot}$ , and orbital period = 16.68 d, in Jonker et al. (2007). We also adopted  $\alpha = 0.1-1$ ,  $L_X = 10^{37}$  erg s $^{-1}$ , and  $f \sim 0.9$  ( $r_{\text{in}}/r \sim 1/100$ ). The typical stellar wind velocity is between the horizontal dotted lines. Here, we adopted the typical value of  $V_W = V_{\text{inf}} \times (1 - R/d)^{\beta}$ , where  $V_{\text{inf}}$  is the terminal velocity;  $(1-2) \times 10^8$  cm s $^{-1}$ ,  $\beta = 0.8$ , and  $R/d = 0.54$ . We adopted the radius of the companion star,  $R$ , as that of the Roche lobe ( $=1.3 \times 10^{12}$  cm) at periastron, although the radius is a little smaller than that derived by spectral classification (B5-A0I) (Jonker et al. 2007). The left solid lines are  $\dot{M}_c = 10^{-5}M_{\odot}\text{yr}^{-1}$  and the right dashed lines are  $\dot{M}_c = 10^{-6}M_{\odot}\text{yr}^{-1}$ . A set of two lines indicate when  $\alpha = 1$  and 0.1. Here, the vertical dotted line indicates the estimated typical outer disk radius assuming the exponential decay model ( $\sim 5 \times 10^{10}$  cm). To the right of solid and dashed lines, the conditions for wind stripping are fulfilled. Figure 7 shows that wind stripping works in the case of  $\dot{M}_c = 10^{-5}M_{\odot}\text{yr}^{-1}$  and  $\alpha = 1$ . This means that wind stripping occurs when the mass loss rate is large.

Next, we consider other conditions as follows. For instance, the accretion radius could be larger than that derived from exponential decay model and the ram pressure of the stellar wind is likely about one order of magnitude higher than that of the smooth wind adopted in this paper. As shown in subsection 2.3, we cannot determine whether the decay is exponential or linear. Here, we notice that periastron spikes do not occur in the outbursts with a sudden drop (see figure 1 and table 1). This may indicate that the X-ray irradiation is smaller because there is no spherical accretion onto the neutron star. Then the decay would be more likely to be linear, and the obtained outer radius of the accretion disk can be large ( $\gtrsim 7 \times 10^{10}$  cm), as shown in table 3. This larger radius is also compatible with the resonant radius,  $(4-5) \times 10^{11}$  cm, which is calculated by the method of Artymowicz and Lubow (1994).

Moreover, it is now widely accepted that the wind of OB stars is clumpy. The core density becomes one order of magnitude higher than that in the smooth wind (e.g., Hamann et al. 2008; Puls et al. 2008). With 10 times higher density wind in equation (8), the solid and dashed

lines in figure 7 move to the left, and this change, together with the larger outer radius ( $\gtrsim 7 \times 10^{10}$  cm), makes the wind stripping model consistent with the observations.

Even when the ram pressure of the wind does not exceed the gas pressure on the equatorial plane, it may blow out the surface of the accretion disk. This may cause expansion of the disk followed by a decrease in  $P_g$ . Then the interaction causes a state transition at the outer part of the accretion disk. The luminosity may suddenly drop below the soft-to-hard transition luminosity, that is,  $(3.5 \pm 0.7) \times 10^{36}$  erg s $^{-1}$  (D’Aì et al. 2012), although it is very difficult to confirm that the state transition occurred in the outer disk region in our results.

We also estimated the time scale of propagation of the sudden stripping from the outer disk to the inner disk. The viscous time scale is given by Frank et al. (1992) as

$$t_{\text{visc}} \sim 3 \times 10^5 \alpha^{-4/5} \dot{M}_{16}^{-3/10} M_{1.4}^{1/4} R_{10}^{5/4} \text{ s,} \quad (12)$$

where  $\dot{M}_{16}$  is the mass accretion rate in units of  $10^{16}$  g s $^{-1}$ , and  $R_{10}$  is the typical length scale for surface density changes in the disk in units  $10^{10}$  cm. Here, we assume  $\alpha = 0.1-1$ ,  $\dot{M}_{16} = 5.3$  ( $L_x \sim 10^{37}$  erg s $^{-1}$ ),  $M_{1.4} = 1$ , and  $R_{10} \sim 0.5$  (the radius after wind stripping, which is one order of magnitude smaller than the typical outer radius assuming the exponential decay), and we find  $t_{\text{visc}} \sim 1-6$  d. The time scale is longer than that of sudden drop (a few hours). However, if wind stripping occurs during the dip of phase 0.95–1.3, the time scale is consistent with the observations.

#### 4. Conclusion

Out of 21 outbursts observed with MAXI/GSC, 7 showed sudden luminosity decreases around periastron, which led to the end of the outburst. The light curve of the decay part can be fitted as well by either a single linear function or a single exponential function. We investigated three interpretations for the sudden end of the outburst around periastron: (1) the end of the outburst during the dip, (2) the propeller effect, and (3) the stripping effect by the stellar wind of the companion star. (1) is possible for only two outbursts, assuming linear decay. (2) is not plausible because a luminosity significantly higher than 1%–4% of the Eddington luminosity is required for a state transition. If the inner disk is truncated, however, it is possible for the transition to occur at a higher luminosity, and the sudden drop can be explained by the propeller effect. However, it is very difficult to confirm the disk truncation in our results, although the variability in the luminosity before the sudden drop suggests instability in the inner disk. Finally, it is also difficult to explain the sudden drop by (3) if a large mass loss rate is not assumed. However, in the case of wind clumping and/or large outer radius assuming linear decay, it is possible for the wind stripping to trigger the sudden end of the outburst. The interaction may cause the state transition at the outer part of the accretion disk. As a result, the luminosity may suddenly drop below the soft-to-hard transition luminosity,  $(3.5 \pm 0.7) \times 10^{36}$  erg s $^{-1}$ .

We would like to acknowledge the MAXI team for MAXI operation and for watching and analyzing real time data. We also would like to acknowledge Toshihiro Takagi for his elaborate analysis of milli-second pulsation search of Cir X-1. This research was partially supported by the Ministry of Education, Culture, Sports, Science and Technology (MEXT), Grant-in-Aid for Science Research 24340041.

## References

- Armstrong, R. P., et al. 2013, MNRAS, 433, 1951  
 Artymowicz, P., & Lubow, S. H. 1994, ApJ, 421, 651  
 Asai, K., et al. 2012, PASJ, 64, 128  
 Asai, K., et al. 2013, ApJ, 773, 117  
 Barthelmy, S. D., et al. 2005, Space Sci. Rev., 120, 143  
 Boutloukos, S., van der Klis, M., Altamirano, D., Klein-Wolt, M., Wijnands, R., Jonker, P. G., & Fender, R. P. 2006, ApJ, 653, 1435  
 Burderi, L., di Salvo, T., Robba, N. R., del Sordo, S., Santangelo, A., & Segreto, A. 1998, ApJ, 498, 831  
 Brandt, W. N., Fabian, A. C., Dotani, T., Nagase, F., Inoue, H., Kotani, T. & Segawa, Y. 1996, MNRAS, 283, 1071  
 Bradt, H. V., Rothschild, R. E., & Swank, J. H. 1993, A&AS, 97, 355  
 Brandt, W. N., & Schulz, N. S. 2000, ApJ, 544, L123  
 Campana, S., Colpi, M., Mereghetti, S., Stella, L., & Tavani, M. 1998 A&A Rev., 8, 279  
 Campana, S., Coti Zelati, F., & D'Avanzo, P. 2013, MNRAS, 432, 1695  
 Campana, S., Stella, L., & Kennea, J. A. 2008, ApJ, 684, L99  
 Campana, S., Stella, L., Mereghetti, S, Colpi, M., Tavani, M., Ricci, D., Fiume, D. Dal, & Belloni, T. 1998, ApJ, 499, L65  
 Clarkson, W. I., Charles, P. A., & Onyett, N. 2004, MNRAS, 348, 458  
 D'Ai, A., et al. 2012, A&A, 543, 20  
 Frank, J., King, A., & Raine, D. 1992, Accretion power in astrophysics. (Camb. Astrophys. Ser., Vol. 21)  
 Gehrels, N., et al. 2004, ApJ, 611, 1005  
 Gierliński, M., Done, C., & Page, K. 2008, MNRAS, 388, 753  
 Ghosh, P., & Lamb, F. K. 1979, ApJ, 232, 259  
 Hamann, W.-R., Feldmeier, A., & Oskinova, L. M. 2008, Clumping in Hot-Star Winds  
 Heinz, S., et al. 2013, ApJ, 779, 171  
 Iaria, R., Burderi, L., Di Salvo, T., La Barbera, A., & Robba, N. R. 2001a, ApJ, 547, 412  
 Iaria, R., Di Salvo, T., Burderi, L., & Robba, N. R. 2001b, ApJ, 561, 321  
 Jonker, P. G., Nelemans, G., & Bassa, C. G. 2007, MNRAS, 374, 999  
 Johnston, H. M., Fender, R., & Wu, K. 1999, MNRAS, 308, 415  
 Kaluzienski, L. J., Holt, S. S., Boldt, E. A., & Serlemitsos, P. J. 1976, ApJL, 208, L71  
 Kato, S., Fukue, J., & Mineshige, S. 1998, Black-hole accretion disks. Edited by Shoji Kato, Jun Fukue, and Sin Mineshige. Publisher: Kyoto, Japan: Kyoto University Press, 1998. ISBN: 4876980535  
 King, A. R., & Ritter, H. 1998, MNRAS, 293, L42  
 Kirsch, M. G., et al. 2005, Proc. SPIE, 5898, 22  
 Lasota, J.-P. 2001, New Astronomy Reviews, 45, 449  
 Levine, A. M., et al. 1996, ApJL, 469, L33  
 Lin, D., Remillard, R. A., Homan, J., & Barret, D. 2012, ApJ, 756, 34  
 Linares, M., et al. 2010, ApJL, 719, L84  
 Matsuoka, M., et al. 2009, PASJ, 61, 999  
 Matsuoka, M., & Asai, K. 2013, PASJ, 65, 26  
 Maccarone, T. J. 2003, A&A, 409, 697  
 Mihara, T., et al. 2011, PASJ, 63, S623  
 Mohamed, S., & Podsiadlowski, P. 2007, 15th European Workshop on White Dwarfs, 372, 397  
 Nakajima, M., et al. 2010, The Astronomer's Telegram, 2608  
 Negoro, H., et al. 2010, ASPC, 434, 127N  
 Nicolson, G. D. 2007, The Astronomer's Telegram, 985, 1  
 Parkinson, P. M. S., et al. 2003, ApJ, 595, 333  
 Powell, C. R., Haswell, C. A., & Falanga, M. 2007, MNRAS, 374, 466  
 Puls, J., Vink, J. S., & Najarro, F. 2008, A&A Rev., 16, 209  
 Shirey, R. E., Bradt, H. V., & Levine, A. M. 1999a, ApJ, 517, 472  
 Shirey, R. E., Levine, A. M., & Bradt, H. V. 1999b, ApJ, 524, 1048  
 Soleri, P., Tudose, V., Fender, R., van der Klis, M., & Jonker, P. G. 2009, MNRAS, 399, 453  
 Sugizaki, M., et al. 2011, PASJ, 63, S635  
 Tennant, A. F., Fabian, A. C., & Shafer, R. A. 1986, MNRAS, 221, 27  
 Tomida, H., et al. 2011, PASJ, 63, 397  
 Wang, Y.-M. 1997, ApJ, L475, L135  
 White, N. E. 1989, A&A Rev., 1, 85